Electronic Supplementary Material (ESI) for Analytical Methods.


# Supporting information

# A voltammetric sensor based on reduced graphene oxide/*β*-cyclodextrin/silver nanoparticle/polyoxometalate nanocomposite for detecting uric acid and tyrosine

Xu Chai[a], Yongbiao Li[a], Chaonan Ma[a], Minjie Guo[a], Zhi Fan[a], Jin Zhao[a,*], Bowen Cheng[a,*]

[a] *Tianjin Key Laboratory of Brine Chemical Engineering and Resource Eco-utilization, College of Chemical Engineering and Materials Science, Tianjin University of Science & Technology, Tianjin 300457, P.R. China*

*zhaoj@tust.edu.cn; zhaoj614@126.com*

**Section 1. Synthesis of RGO- POM**

GO (1 mg/mL, 6.66 mL) were dispersed in deionized water (10 mL) under ultrasonification. Then, $H_3PW_{12}O_{40}$ (88 mg/mL, 4 mL) and isopropanol (700 $\mu$L) were added into the above suspension. The suspension was irradiated by UV light for 60 min, and then filtered to obtain the target electrode material.

**Section 2. Synthesis of RGO-CD-POM**

GO (1 mg/mL, 6.66 mL), $\beta$-CD (1 mg/mL, 0.66 mL) was dispersed in deionized water (9mL) under ultrasonification. Then, $H_3PW_{12}O_{40}$ (88 mg/mL, 4 mL) and isopropanol (700 $\mu$L) were added into the above suspension. The suspension was irradiated by UV light for 60 min, and then filtered to obtain the target electrode mater.

**Section 3. Synthesis of RGO-AgNP-POM**

GO (1 mg/mL, 6.66 mL), AgNP $AgNO_3$ (2.22 mg/mL, 3 mL) was dispersed in deionized water (8mL) under ultrasonification. Then, $H_3PW_{12}O_{40}$ (88 mg/mL, 4 mL) and isopropanol (700 $\mu$L) were added into the above suspension. The suspension was irradiated by UV light for 60 min, and then filtered to obtain the target electrode mater.

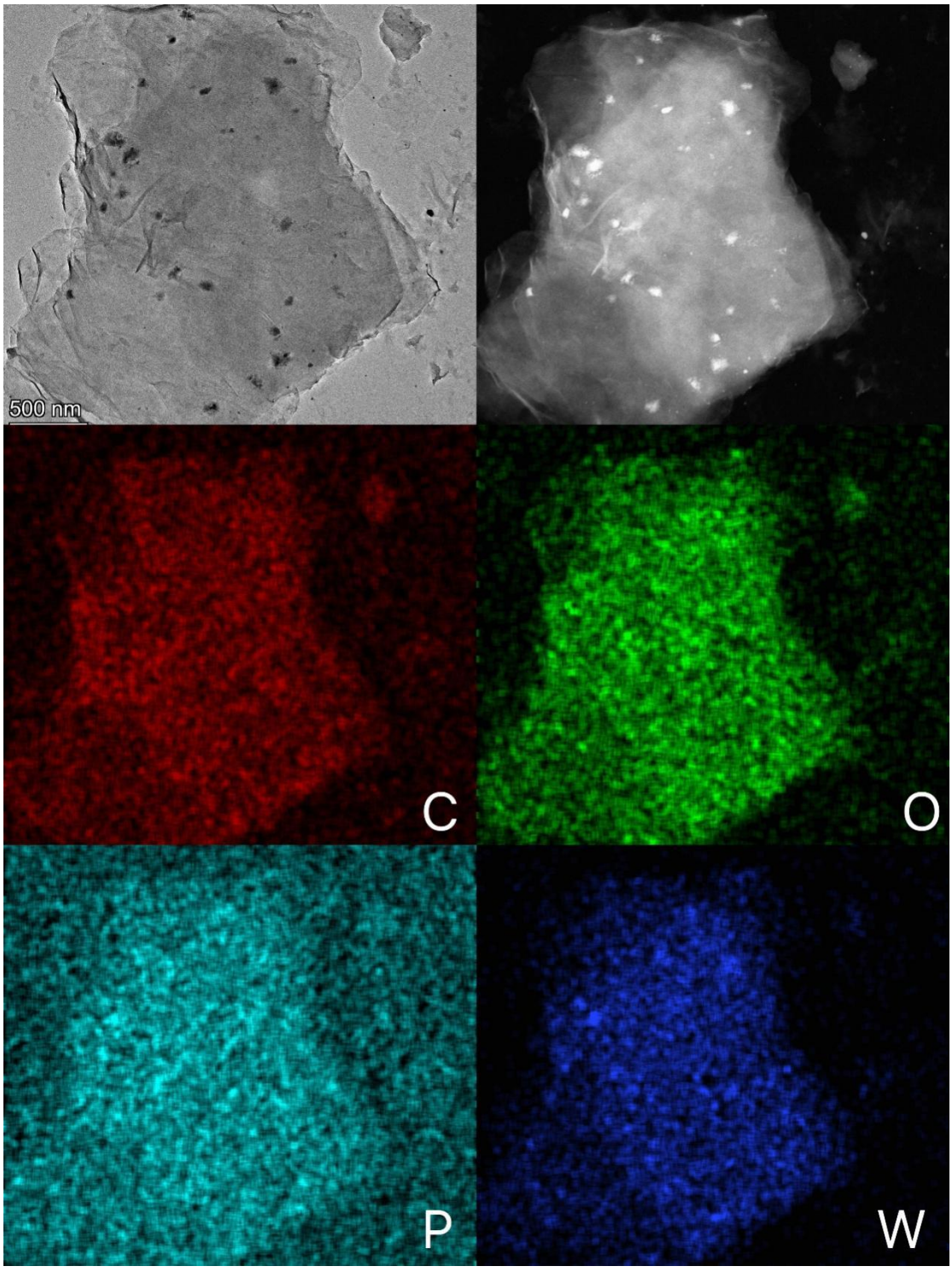


**Figure S1.** TEM-EDS mapping images of RGO-POM hybrid.

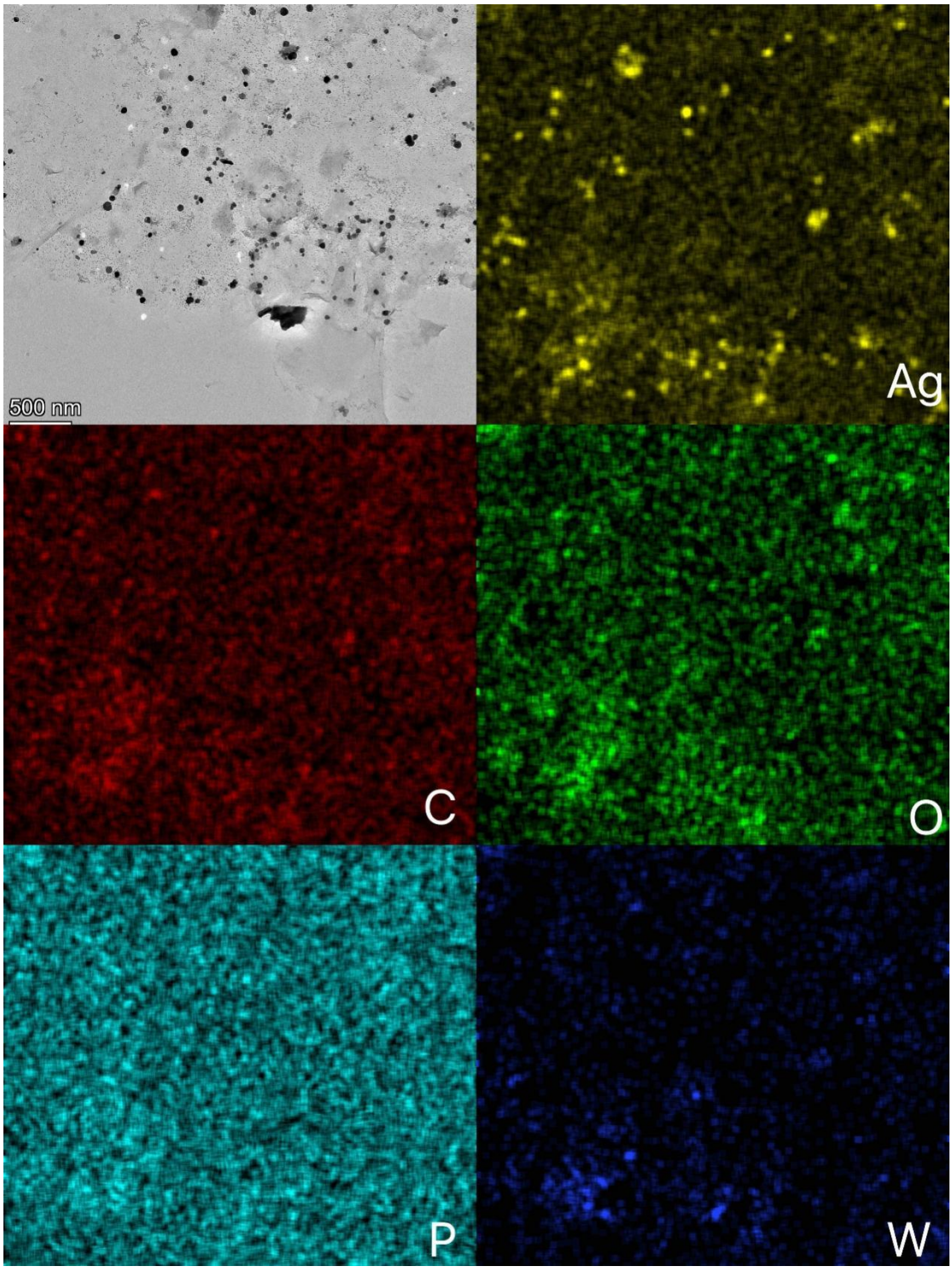


**Figure S2.** TEM-EDS mapping images of RGO-AgNP-POM hybrid.

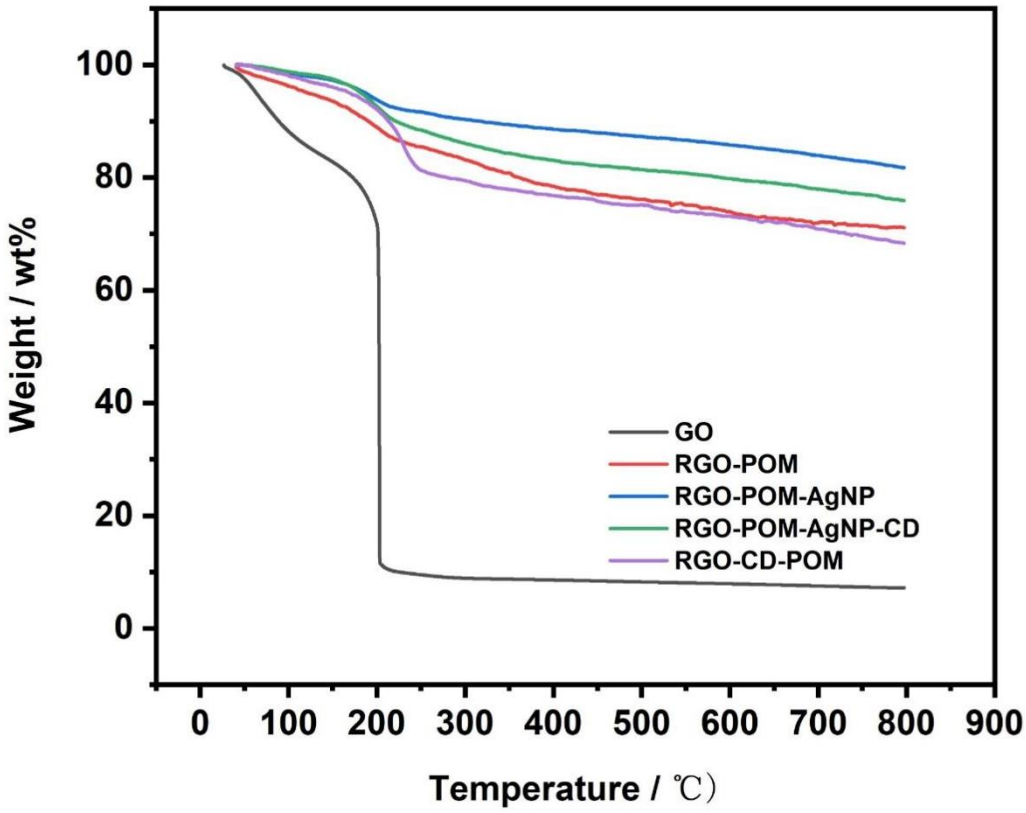


**Figure S3.** TGA curves of GO, RGO-POM, RGO-AgNP-POM, RGO-CD-POM and RGO-CD-AgNP-POM

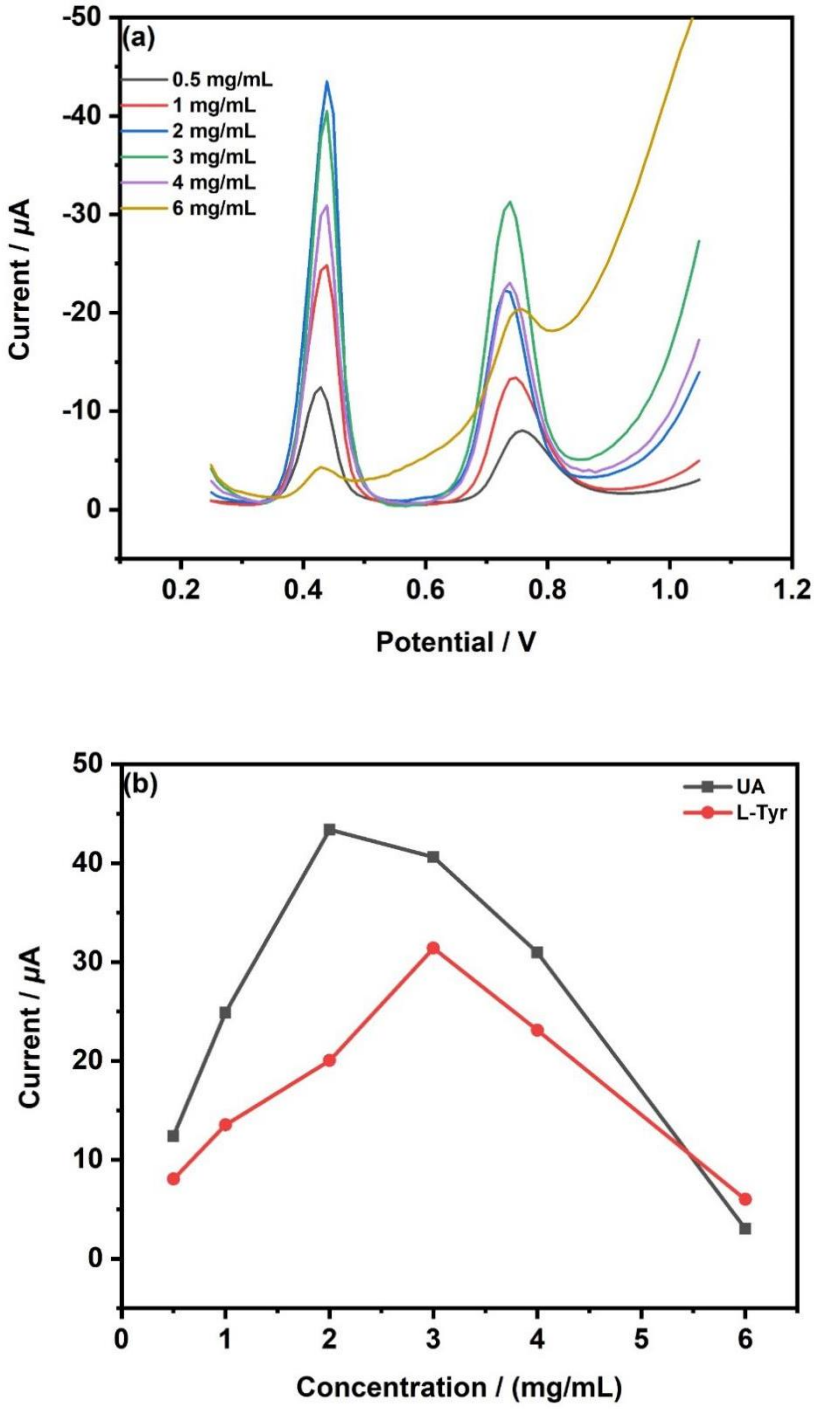


**Figure S4.** DPV curves for 500 $\mu$M UA, 400 $\mu$M L-Try mixed solution at RGO-CD-AgNP-POM/GCE with different dispersion concentration (a) and effect of the amount of RGO-CD-AgNP-POM/GCE on peak current(b)

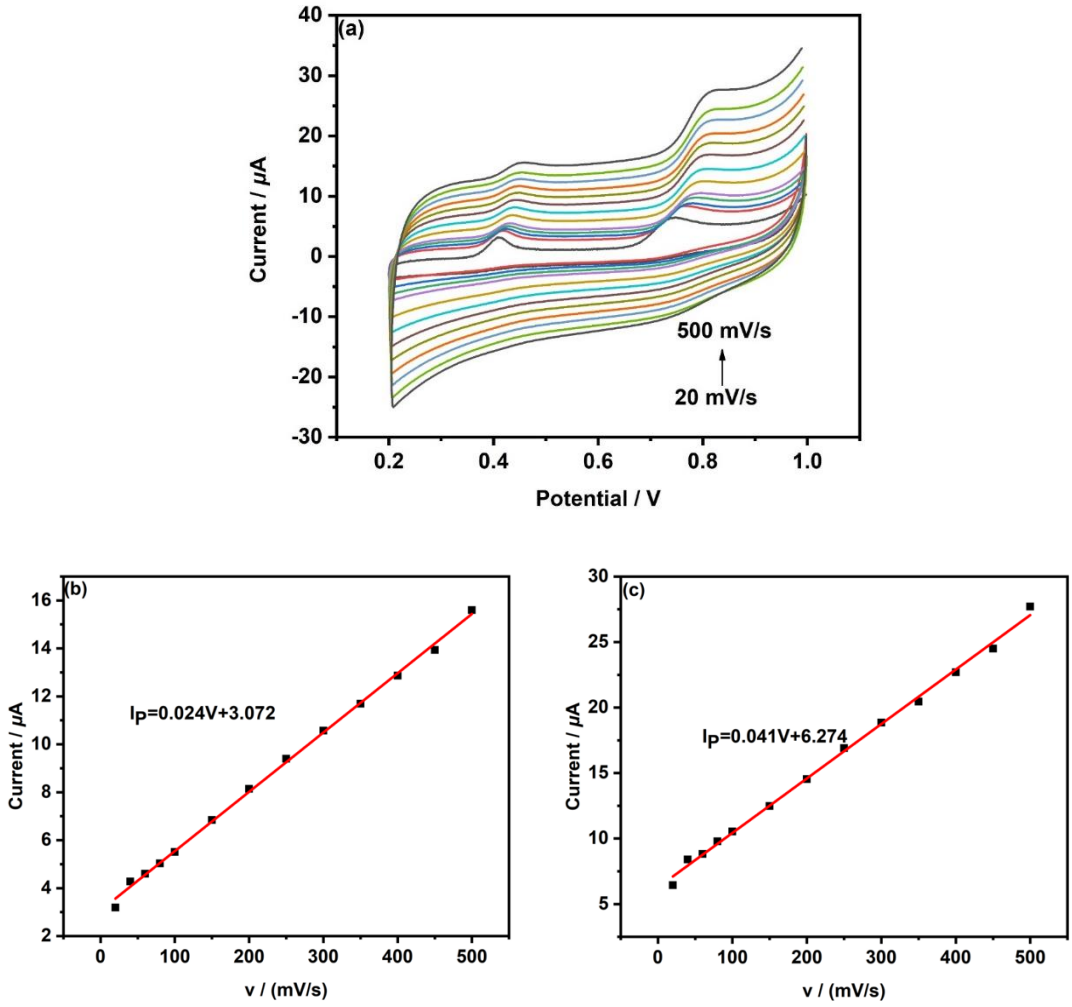


**Figure S5.** (a) Cyclic voltammograms in the presence of 150 $\mu$M UA and 200 $\mu$M L-Tyr mixture in different scan rate (20~500 mV/s) at RGO-CD-AgNP-POM/GCE in phosphate buffer solution (pH 6.0). The plots of Ip vs v for (b) UA (c) L-Tyr.

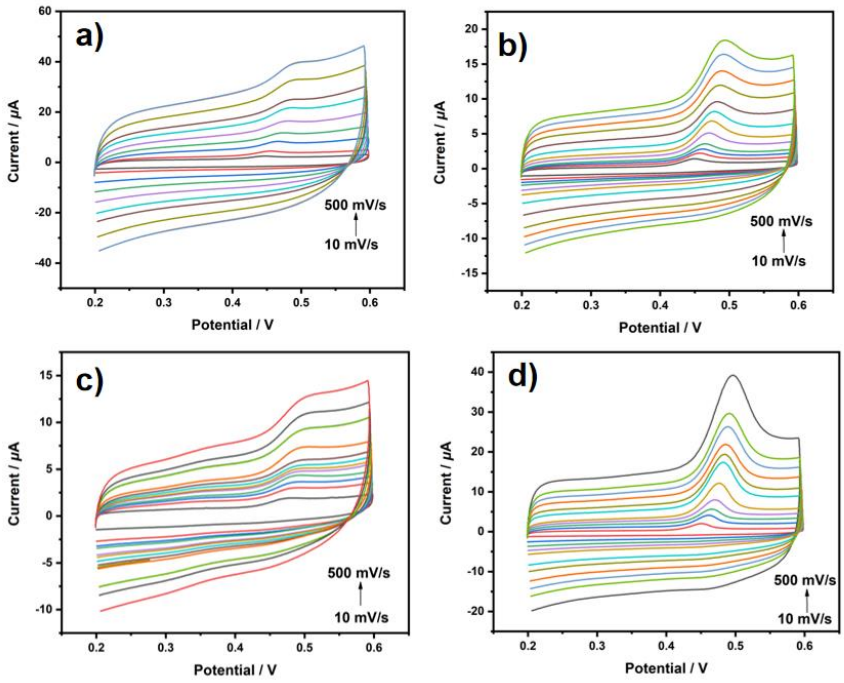


**Figure S6.** Cyclic voltammograms in the presence of 150 $\mu$M UA in different scan rate (10~500 mV/s) at RGO-POM/GCE(a), RGO-CD-POM/GCE(b) RGO-AgNP-POM/GCE(c) and RGO-CD-AgNP-POM/GCE(d) in phosphate buffer solution (pH 6.0).

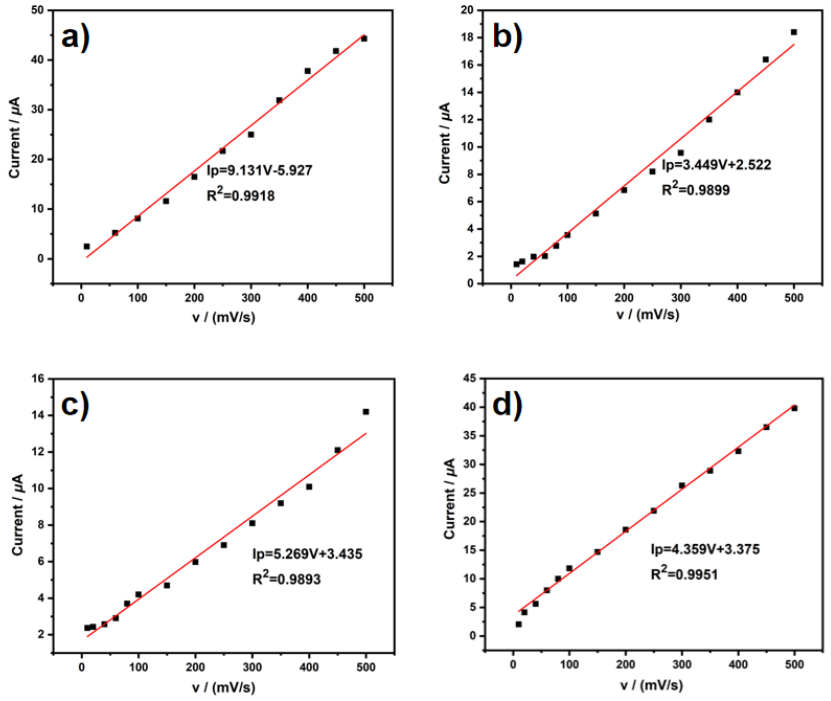


**Figure S7.** A Plot of peak current against of scan rate at RGO-POM/GCE(a), RGO-CD-POM/GCE(b) RGO-AgNP-POM/GCE(c) and RGO-CD-AgNP-POM/GCE(d).

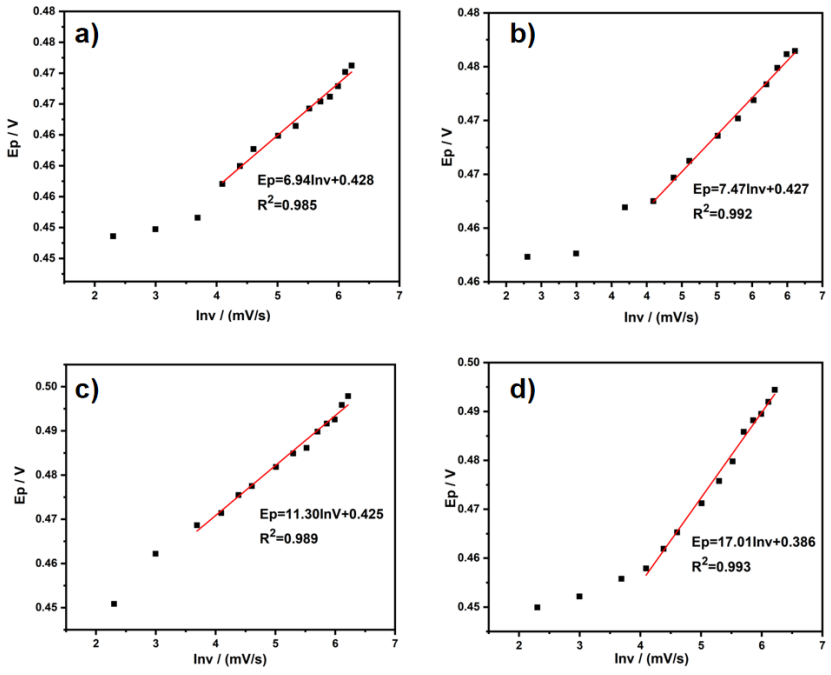


**Figure S8.** A plot of potential against lnv at RGO-POM/GCE(a), RGO-CD-POM/GCE(b), RGO-AgNP-POM/GCE(c) and RGO-CD-AgNP-POM/GCE(d).

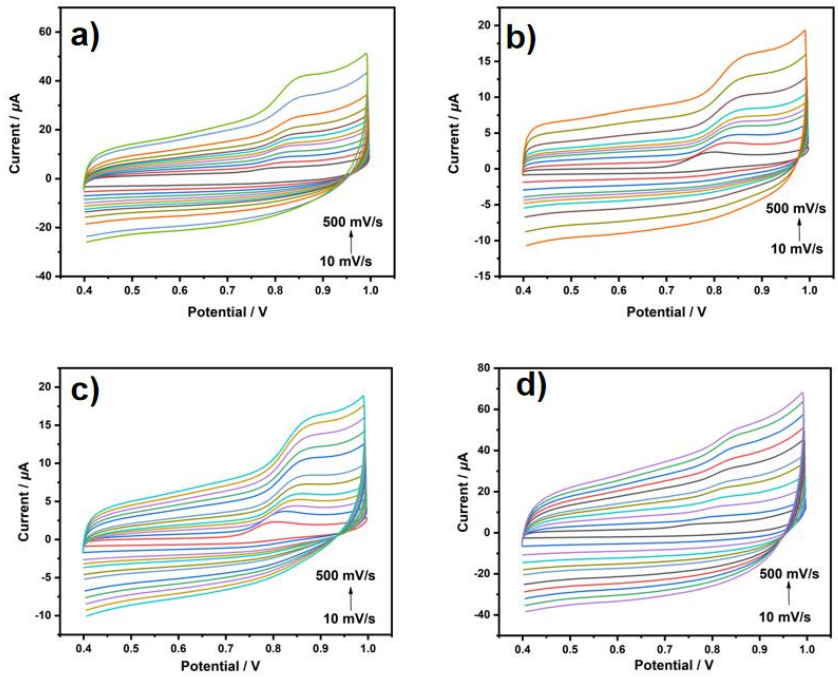


**Figure S9.** (a) Cyclic voltammograms in the presence of 200 $\mu$M L-Tyr in different scan rate (10~500 mV/s) at RGO-POM/GCE(a), RGO-CD-POM/GCE(b) RGO-AgNP-POM/GCE(c) and RGO-CD-AgNP-POM/GCE(d) in phosphate buffer solution (pH 6.0).

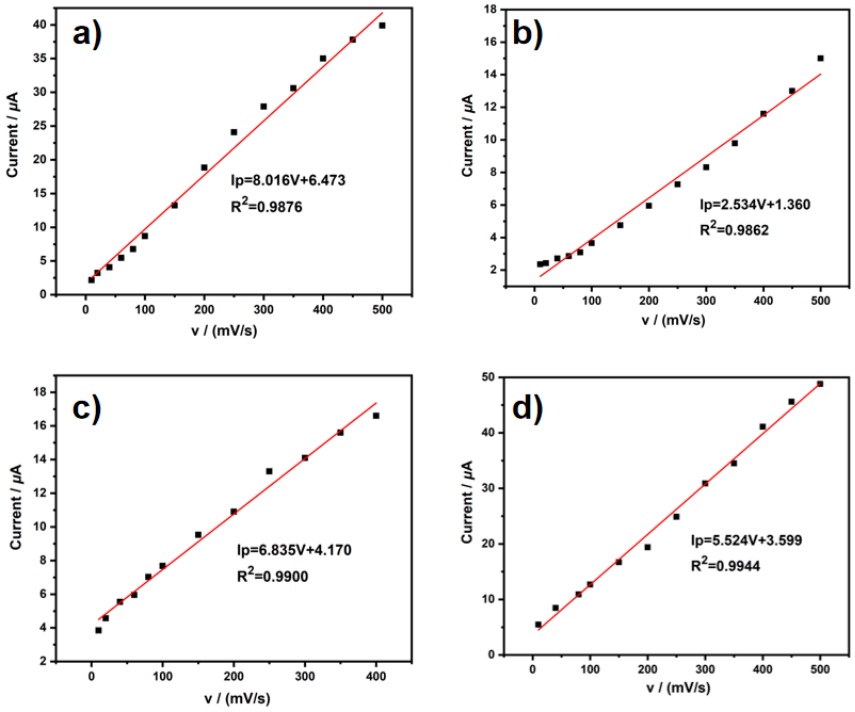


**Figure S10.** A Plot of peak current against of scan rate at RGO-POM/GCE(a), RGO-CD-POM/GCE(b), RGO-AgNP-POM/GCE(c) and RGO-CD-AgNP-POM/GCE(d).

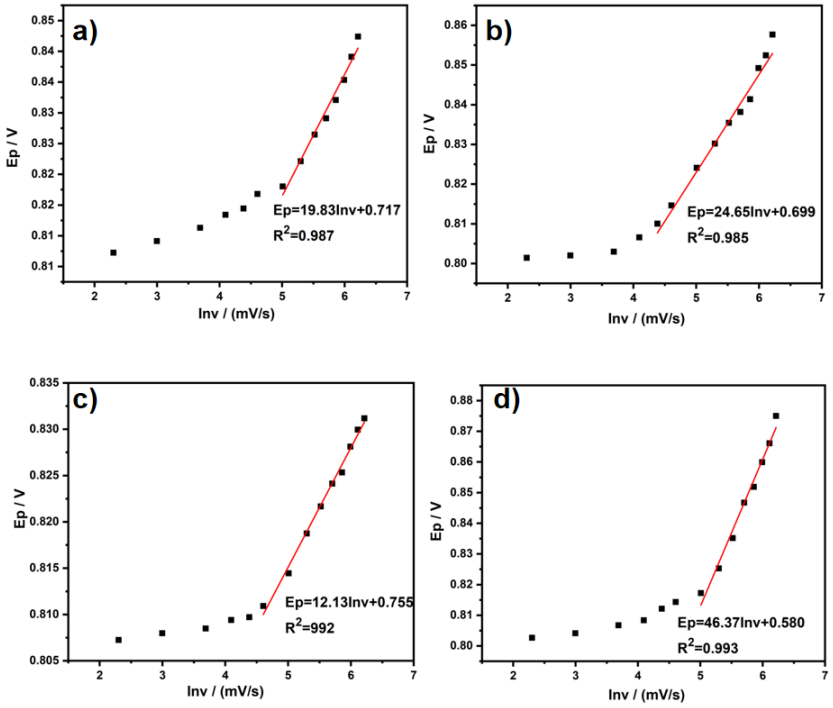


**Figure S11.** A plot of potential against lnv at RGO-POM/GCE(a), RGO-CD-POM/GCE(b), RGO-AgNP-POM/GCE(c) and RGO-CD-AgNP-POM/GCE(d).

Modified electrode materials are crucial in improving the electrochemical sensing performance of electrodes, with the mass transfer and diffusion process of modified electrodes determining their performances. To obtain physicochemical characteristic information of the modified electrodes surfaces, the effect of scanning rate (v) on the electrochemical behaviors was investigated by CV experiments in 150 $\mu$M UA solution at RGO-POM/GCE, RGO-CD-POM/GCE, RGO-AgNP-POM/GCE and RGO-CD-AgNP-POM/GCE (Figure S6). The relationship between peak current (Ip) and scanning rate (ν) were explored (Figure S7). The results showed that Ip was correlated with ν, which indicated that the oxidation of UA at these modified electrodes were adsorption-controlled processes. With the increase of scanning rate, the oxidation peak potentials shifted in the positive direction. Figure C4 shows the linear relationship between the oxidation peak potentials ($E_P$) and the logarithm of the scanning rate (lnν) in the scanning rate range of 150 ~ 500 mV/s (Figure S8). As for L-Tyr, the similar phenomena were observed. The oxidation of L-Tyr at RGO-CD-AgNP-POM/GCE was also an adsorption-controlled process. The linear relationship between $E_P$ and lnν was also observed (Figure S9-S11).

Based on the plots of $E_P$ against lnν, the number of electrons transferred (n) and the electron transfer rate ($k_s$) could be calculated according to Laviron's theory.

$$E_{pa} = E^o + \frac{RT}{(1-\alpha)nF}\ln\left[\frac{RTk_s}{(1-\alpha)nF}\right] - \frac{RT}{(1-\alpha)nF}\ln\nu \qquad \textbf{(1)}$$

Based on equation (1), we can infer that the range of n is 2.28-5.32 (in general, considering 0.3< α <0.7). According to previous literatures, it can be inferred that UA and L-Tyr lose two electrons respectively. Therefore, the electrochemical oxidation

mechanisms of UA and L-Tyr at RGO-CD-AgNP-POM/GCE are shown as follows:

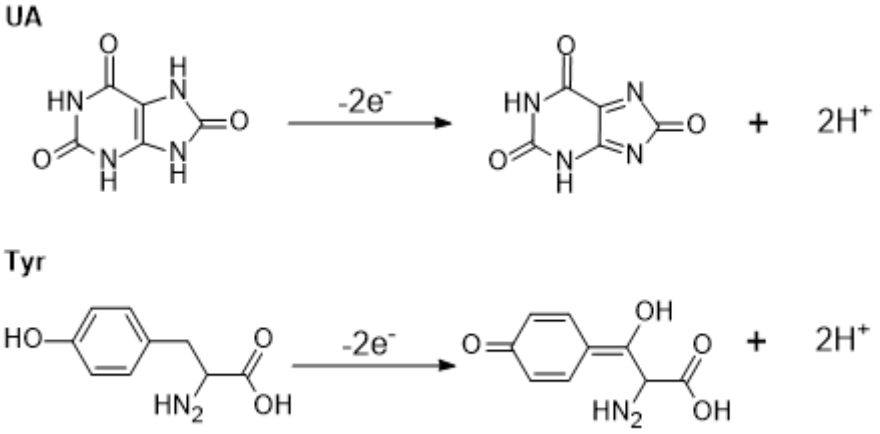


The electron transfer rate constant ($k_s$) can be obtained according to equation (2):

$$k_s = \frac{\alpha n F v}{RT} \qquad \textbf{(2)}$$

Where, $\alpha$ is charge transfer coefficient; n is number of electron transfer; F is Faraday constant (96485 C/mol); R is ideal gas constant (8.3144 J/mol·K); T is temperature (298 K); v is scanning rate;

From equation (2), it can be deduced that $k_s$ is proportional to α. Therefore, the bigger α, the bigger $k_s$. From the greater slopes, it can be concluded that the electron transfer rates of UA and L-Tyr at RGO-CD-AgNP-POM/GCE are higher than those at other modified electrodes (Figure S8 & S11). Therefore, RGO-CD-AgNP-POM can effectively promote the electron transfer process on the heterogeneous interface.

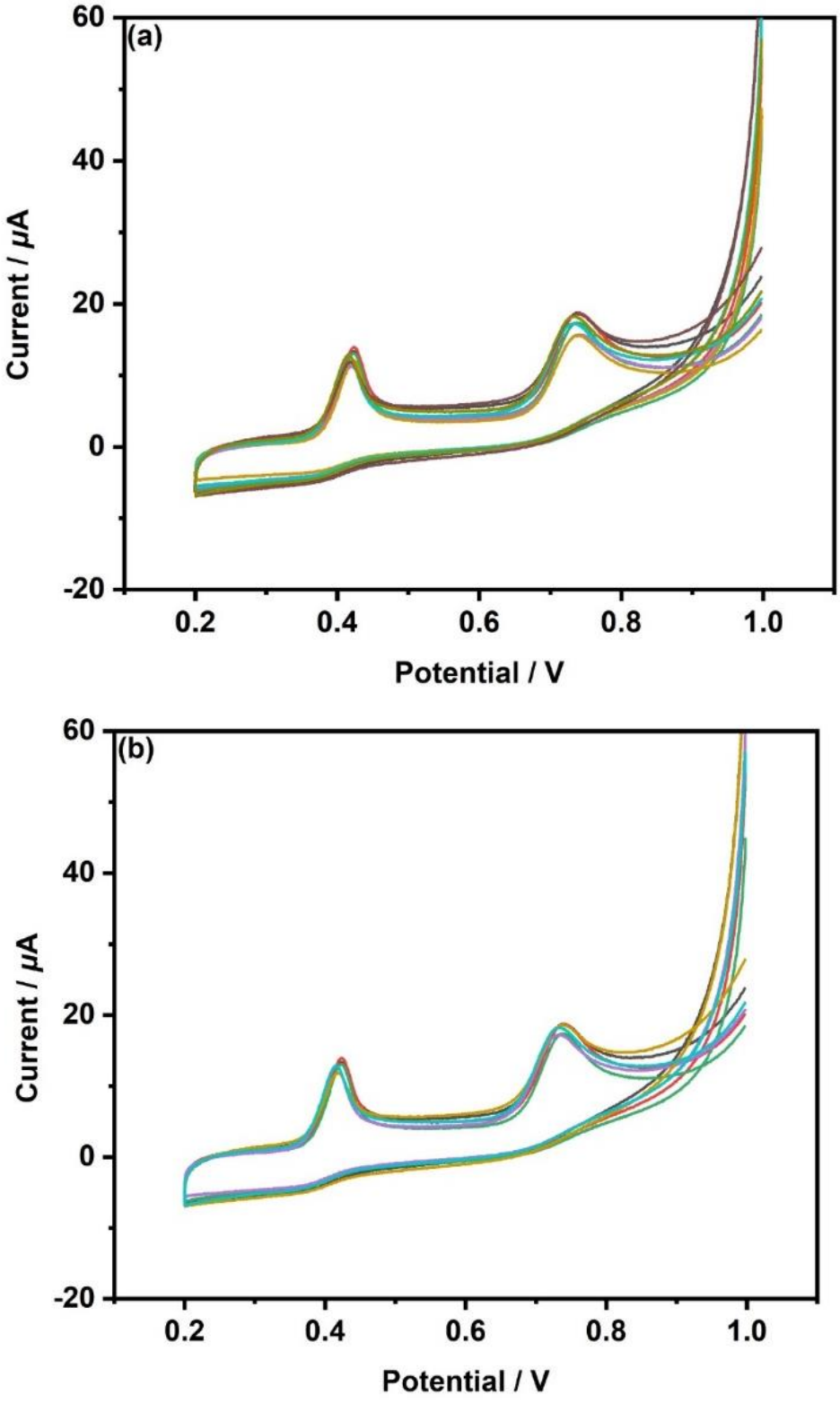


**Figure S12.** CV curves for150 $\mu$M UA and 200 $\mu$M L-Tyr at 6 independently RGO-CD-AgNP-POM/GCE (a); CV curves for 150 $\mu$M UA and 200 $\mu$M L-Tyr at RGO-CD-AgNP-POM/GCE for a week (b).

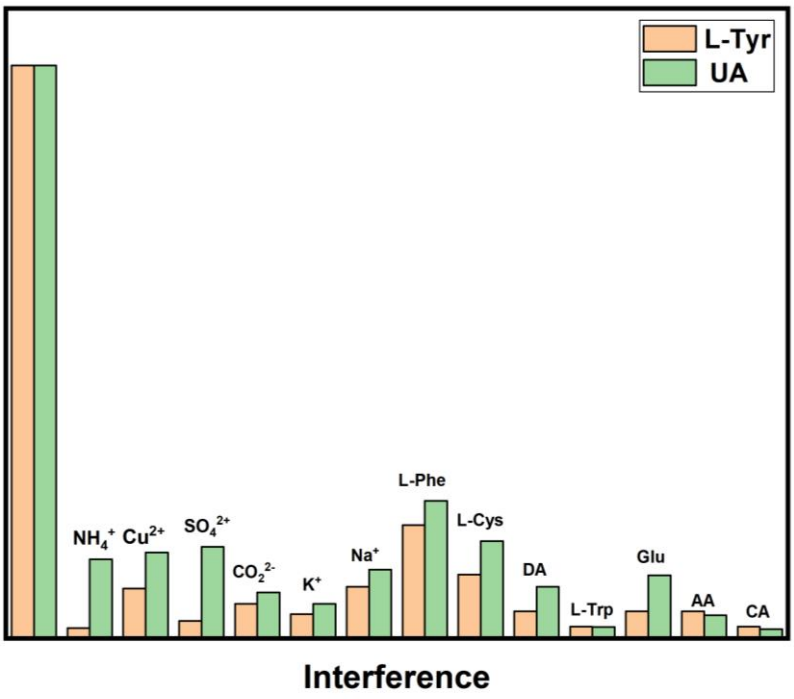


**Figure S13.** Interference studies at RGO-CD-AgNP-POM/GCE.